Computers and Concrete, Vol. 5, No. 3 (2008) 195-216
DOI: http://dx.doi.org/10.12989/cac.2008.5.3.195

Hypoelastic modeling of reinforced concrete walls

Mohsen A. Shayanfar*

Civil Engineering Department, Iran University of Science and Technology, Narmak 16846, Tehran, Iran

Amir Safiey‡

Moshanir Power Engineering Consultants, Park Prince Buildings, Vanak, Tehran, Iran

(Received February 27, 2007, Accepted May 6, 2008)

Abstract. This paper presents a new hypoelasticity model which was implemented in a nonlinear finite element formulation to analyze reinforced concrete (RC) structures. The model includes a new hypoelasticity constitutive relationship utilizing the rotation of material axis through successive iterations. The model can account for high nonlinearity of the stress-strain behavior of the concrete in the pre-peak regime, the softening behavior of the concrete in the post-peak regime and the irrecoverable volume dilatation at high levels of compressive load. This research introduces the modified version of the common application orthotropic stress-strain relation developed by Darwin and Pecknold. It is endeavored not to violate the principal of "simplicity" by improvement of the "capability". The results of analyses of experimental reinforced concrete walls are presented to confirm the abilities of the proposed relationships.

Keywords: cracking; damage; smeared crack model; hypoelasticity; strength degradation; shear wall.

1. Introduction

In recent years, a large number of constitutive models for concrete materials have been developed, but the models that are rational, reliable, practical and simple to implement in a general purpose finite element analysis program are very limited. A rational concrete model should be able to describe adequately the main characteristics of the complete stress-strain behavior of concrete materials, ranging from a tension with a low confining pressure to a compressive state with very high confining pressure, besides dealing with both the pre-peak and the post-peak regimes; furthermore, the reliability of an applicable model is closely related to its numerical stability, which in turn depends on its formulation and the numerical techniques adopted for its computer implementation. This practical application requires that the model should be as simple as possible, as long as the main characteristics of the constitutive behavior of the concrete materials are "captured". The main characteristics of a proper model for concrete materials can be summarized as follows:

(i) The high nonlinearity of the stress-strain behavior of concrete in the pre-peak regime, i.e., growing and propagation of micro-cracks resulting in a decrease in the material stiffness.

* Faculty Member, E-mail: mohsenalishayanfar@gmail.com
‡ Engineer, E-mail: a_safiey@yahoo.com

(ii) The softening behavior of concrete in the post-peak regime resulting from the localization of macro-cracks in narrow bands.

(iii) The irrecoverable volume dilatation at high level of compressive load resulting in an increase in the Poisson's ratio.

All of the above features for concrete are included in the material model developed during this course of study. This model can be treated as a hypoelastic model which is very simple to implement in a nonlinear finite element analysis program. The incremental nature of the hypoelastic models along with the nonlinear stress-strain relationship utilized in the proposed model, capture the nonlinear stress-strain behavior of concrete. The proposed constitutive model is applicable for the entire stress or strain history including the post-peak regions and can model the strain softening behavior of concrete through the assumed nonlinear stress-strain curve. A variable Poisson's ratio is used to account for volume dilatation at high stress levels.

In the followings, a brief review on the objective of the reinforced concrete constitutive models is stated. Afterwards, the proposed analytical model will be introduced in detail. Eventually, the analytical procedure is verified by a set of numerical analysis, consisting of shear panel W-2 tested by Cervenka (1970), squat shear walls, namely DP1 and DP2, tested by Palermo and Vecchio (2002), and SW shear walls tested by Lefas, *et al.* (1990).

2. Review of constitutive models for concrete

Extensive research over the past decades has led to a few constitutive models for concrete which are based on the principles of continuum mechanics and neglect the microstructure of the concrete. These include elasticity-based models, plasticity-based models, plastic-fracturing models, elastic-plastic-damage models, and the endochronic model (ASCE 1982). Elasticity-based models are among the most popular constitutive relationships used in conjunction with the finite element analysis of concrete structures. These models are simple and can be easily formulated and implemented. Several elasticity-based constitutive models can be found in the literature, but in general they can be grouped under the following approaches: (i) Linear elastic model; and (ii) Non-linear elastic models. Hypoelastic models are from the second category.

An alternative approach to overcome some deficiency associated to the other linear models is to describe the material behavior in terms of increments of stress and strain. The stress-strain relationships are then expressed using the tangent stiffness which varies with the current stress state. Thus, this class of model is generally dependent on the deformation history. The behavior of this class of model is infinitesimally (or incrementally) reversible (elastic behavior). Literally, "hypo" means "in a lower sense" or "to a lower degree". Hence, hypoelastic can imply a material that is elastic to a lower or incremental sense. A hypoelastic material can be interpreted to be capable of allowing for inelastic or plastic behavior. If the orthotropic models are expressed in terms of increments of stress and strain, they are called hypoelastic models. Some of those include the models proposed by Liu, *et al.* (1972), Darwin and Pecknold (1974), Elwi and Murray (1979), Bathe, *et al.* (1989), Bouzaiene and Massicotte (1997), and Balan, *et al.* (2001). The constitutive models of Liu, *et al.* (1972) and Darwin and Pecknold (1977) are developed as two-dimensional stress-strain relationship while the other constitutive models are developed as three-dimensional stress-strain relationship. The two-dimensional stress-strain relationships are much simpler for implementation into a computer program and adequate for models consisting of the shell element

types; therefore, these types of models would be more widespread in the analytical studies. In this regard, the constitutive law proposed by Darwin and Pecknold (1974) is well recognized among the researchers; although, almost three decades have passed from its invention, but some of the researchers still take the advantage of the model, e.g., refer to a set of studies carried out by Kwak and Kim (2001, 2004a, 2004b). Here, some alterations are proposed to improve the abilities of the constitutive relationship developed by Darwin and Pecknold (1974).

3. Analytical model

3.1. Constitutive model for uncracked concrete

Generalized incremental Hooke's law for an orthotropic material under biaxial loading is as follows:

$$\begin{Bmatrix} d\sigma_{11} \\ d\sigma_{22} \\ d\tau_{12} \end{Bmatrix} = \frac{1}{1-\nu_{12}\nu_{21}} \begin{bmatrix} E_1 & \nu_{21}E_1 & 0 \\ \nu_{12}E_2 & E_2 & 0 \\ 0 & 0 & (1-\nu_{12}\nu_{21})G \end{bmatrix} \begin{Bmatrix} d\varepsilon_{11} \\ d\varepsilon_{22} \\ d\gamma_{12} \end{Bmatrix} \tag{1}$$

Eq. (1) is modified according to the following assumptions: To satisfy the energy conservation principle, the elastic material stiffness matrix should be symmetric, so: $\nu_{21}E_1 = \nu_{12}E_2$. To define the Poisson's ratios (ν_{21}, ν_{12}), it is imposed: $\nu_{21}/E_2 = \nu_{12}/E_1 = \nu/E_0$, where E_0 is the initial stiffness modulus and ν is the equivalent Poisson's ratio. Because of lack of information related to the shear modulus of elasticity of the concrete, G, it is also assumed to be independent of the axis orientation. These assumptions result in $(1-\nu^2E_1E_2/E_0^2)G = 0.25(E_1+E_2-2\nu E_1E_2/E_0)$. At last, the incremental stress-strain relationship in Eq. (1) takes the following form (Shayanfar 1995):

$$\begin{Bmatrix} d\sigma_{11} \\ d\sigma_{22} \\ d\tau_{12} \end{Bmatrix} = \frac{1}{1-\nu^2\dfrac{E_1E_2}{E_0^2}} \begin{bmatrix} E_1 & \nu\dfrac{E_1E_2}{E_0} & 0 \\ \nu\dfrac{E_1E_2}{E_0} & E_2 & 0 \\ 0 & 0 & 0.25\left(E_1+E_2-2\nu\dfrac{E_1E_2}{E_0}\right) \end{bmatrix} \begin{Bmatrix} d\varepsilon_{11} \\ d\varepsilon_{22} \\ d\gamma_{12} \end{Bmatrix} \tag{2}$$

The above constitutive matrix contains four material constants which are the instantaneous tangent stiffness moduli in the principal directions 1 and 2, i.e., E_1 and E_2, the equivalent Poisson's ratio, ν, and the initial modulus of elasticity, E_0. The evaluation of these parameters at each load stage is presented in next sections.

The constitutive matrix should be transformed into the global coordinate system. The reinforcement steel contribution should be added to it; and, finally the element stiffness matrix has to be obtained; formulations of such subjects are discussed in detail elsewhere by Shayanfar (1995). If the angle between the local coordinate system (old system) and the principal coordinate system (new system) is denoted by θ, the constitutive matrix in local coordinate system can be obtained using:

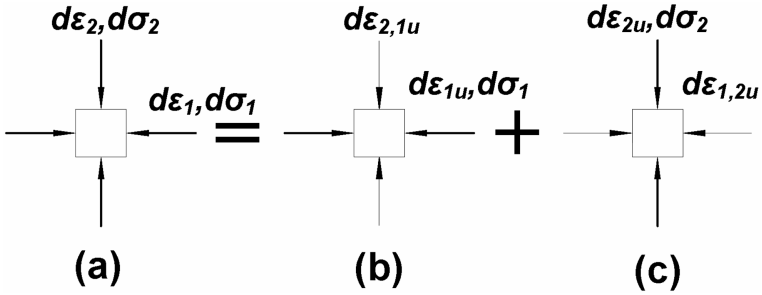

Fig. 1 Schematic representation of real strains and equivalent uniaxial strains

$$[C] = \frac{1}{\left(1-\nu^2\frac{E_1E_2}{E_0^2}\right)}\times\begin{bmatrix} E_1\cos^2\theta+E_2\sin^2\theta & \frac{\nu E_1E_2}{E_0} & \frac{1}{2}(E_1-E_2)\sin\theta\cos\theta \\ & E_1\sin^2\theta+E_2\cos^2\theta & \frac{1}{2}(E_1-E_2)\sin\theta\cos\theta \\ Sym. & & \frac{1}{4}\left(E_1-E_2-2\nu\frac{E_1E_2}{E_0}\right) \end{bmatrix} \quad (3)$$

3.1.1. Equivalent uniaxial strains

The "equivalent uniaxial strain" idea has been adopted as described here. For an increment of stress or strain, the material can be assumed to behave as a linear elastic material and the principle of superposition can be considered to be applicable. Thus, the state of "real" stress at any point of the element in its principal plane is composed of two distinct cases (see Fig. 1):

(i) Stress is applied only along the axis 1 ($d\sigma\neq 0$ and $d\sigma_2 = 0$), and the resulting incremental strains in the principal directions 1 and 2 are ε_{1u} and $\varepsilon_{2,1u}$, respectively (see Fig. 1(b));

(ii) Stress is applied only along the axis 2 ($d\sigma_1 = 0$ and $d\sigma_2\neq 0$), and the resulting incremental strains in principal directions 1 and 2 are $\varepsilon_{1,2u}$ and ε_{2u}, respectively (see Fig. 1(c)).

(iii) The condition for equivalence of the systems (a) and (b+c) is (see Fig. 1):

$$\begin{aligned} d\varepsilon_1 &= d\varepsilon_{1u} + d\varepsilon_{1,2u} \\ d\varepsilon_2 &= d\varepsilon_{2u} + d\varepsilon_{2,1u} \end{aligned} \quad (4)$$

After some mathematical manipulations and using proposed constitutive matrix, the incremental equivalent uniaxial strains, $d\varepsilon_{iu}$, based on the current incremental "real" strains, $d\varepsilon_i$, (i=1,2) relationships can be derived:

$$\begin{Bmatrix} d\varepsilon_{1u} \\ d\varepsilon_{2u} \end{Bmatrix} = \frac{1}{1-\nu^2\frac{E_1E_2}{E_0^2}}\begin{bmatrix} 1 & \frac{\nu E_2}{E_o} \\ \frac{\nu E_1}{E_o} & 1 \end{bmatrix}\begin{Bmatrix} d\varepsilon_1 \\ d\varepsilon_2 \end{Bmatrix} \quad (5)$$

By following a similar procedure, Eq. (5) takes the following form based on Darwin and Pecknold (1974)'s constitutive matrix:

$$\begin{Bmatrix} d\varepsilon_{1u} \\ d\varepsilon_{2u} \end{Bmatrix} = \frac{1}{1-\nu^2} \begin{bmatrix} 1 & \nu\sqrt{\frac{E_2}{E_1}} \\ \nu\sqrt{\frac{E_1}{E_2}} & 1 \end{bmatrix} \begin{Bmatrix} d\varepsilon_1 \\ d\varepsilon_2 \end{Bmatrix} \tag{6}$$

It is obvious that the use of Eq. (6) is limited to the case where the moduli of elasticity (E_1 and E_2) have positive non-zero values. This condition (non-zero value for the modulus of elasticity) occurs when the state of stress in two principal directions is located on the ascending branch of the stress-strain curves. Based on several analyses, it was noticed that when the tangential stiffness, E_i, becomes nearly zero, the error of the incremental equivalent uniaxial strain, $\Delta\varepsilon_{iu}$, resulting from Darwin and Pecknold (1974)'s method ($\Delta\varepsilon_{iu} = \Delta\sigma_i/E_i$) becomes larger, and compression failure of the concrete occurs suddenly with a rapid increase of the equivalent uniaxial strain. On the other hand, the equivalent uniaxial strains evaluated using Eq. (5) does not suffer from the difficulty arising from the division by zero, or a very small value. Therefore, the incremental stress-strain relationship in Eq. (5) is applicable for the entire stress or strain history (in both pre- and post-peak regions), while Eq. (6) can only be used for the pre-peak regime. With the crucial assumption of concrete being an isotropic material, i.e., $E_1 = E_2 = E_0$, Eq. (5) takes the similar form as proposed by Noguchi (ASCE 1985).

3.1.2. Rotation of material axis

During the subsequent iterations/load steps, because of the presence of shear stresses the principal and material axes rotate. The material axes are assumed to coincide with the principal axes. A schematic representation of the material principal axes during two subsequent iterations/load steps is shown in Fig. 2. The orientation of each principal coordinate system is measured with reference to the local coordinate system of the element.

In each iteration/load step, the angle between the current principal coordinate system and the previous coordinate system, $\Delta\theta_i = \theta_{new} - \theta_{old}$, is obtained and then the previous equivalent uniaxial

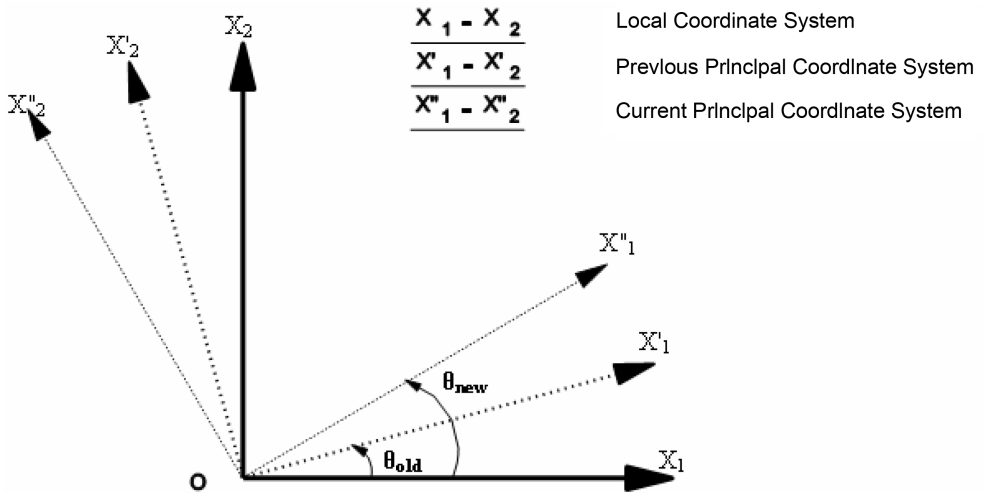

Fig. 2 Schematic representation of different coordinate systems at any point of an element

strain vector is transformed by the angle to obtain its projection in the new principal coordinate system. At last, by performing some mathematical transformations as described by Shayanfar (1995), the new equivalent uniaxial strain vector is calculated. It can be proved based on the above concept, the equivalent uniaxial strain is obtained from the "real" principal strains and the material parameters (and) corresponding to the previous load stage. In Darwin and Pecknold (1974)'s model, the material axes are not transformed if the principal axis rotates within ±45 degrees from their original position; beyond this limit, the material axes are transformed. This method introduces a discontinuity in the computed equivalent uniaxial strains and causes more errors in the computation process (ASCE 1985). The method adopted in this study as outlined earlier, ensures the continuity of the computed equivalent uniaxial strains and gives more reliable results.

3.2. Constitutive model for cracked concrete

Cracking of concrete is one of the important aspects of material nonlinear behavior of concrete. Intensive research effort has resulted in a large number of cracking models, which can be divided broadly into two categories, namely, discrete cracking models and smeared cracking models. Furthermore, within each category, these models can be applied either with a strength-based, or fracture mechanics based crack propagation criterion. The relatively simple strength-based smeared cracking model is a good choice for modeling of cracked RC elements when the global behavior of the structure is to be studied. Also, this model could be used successfully in studying the local behavior of the reinforced concrete elements.

3.2.1. Smeared crack model

The smeared crack model developed by Rashid (1968) has been adopted by the majority of investigators in the area of nonlinear finite element analysis of reinforced concrete structures. This model offers automatic generation of cracks, without a redefinition of the finite element topology and complete generality in possible crack direction. Based on this procedure, the cracked concrete is represented as an orthotropic material with an infinite number of parallel fissures across that part of the finite element. After cracking has occurred (usually defined when the principal tensile stress or strain exceeds a predefined limiting value), the constitutive matrix is defined as:

$$\begin{Bmatrix} d\sigma_1 \\ d\sigma_2 \\ d\tau_{12} \end{Bmatrix} = \begin{bmatrix} E_1 & 0 & 0 \\ 0 & E_2 & 0 \\ 0 & 0 & \beta' G \end{bmatrix} \begin{Bmatrix} d\varepsilon_1 \\ d\varepsilon_2 \\ d\gamma_{12} \end{Bmatrix} \tag{7}$$

In which $E_1 (E_1 = 0)$ and E_2 are the tangential stiffnesses perpendicular and parallel to the crack direction, respectively. Once the second crack is detected in the direction perpendicular to the first crack, the tangential stiffnesses E_2 is also set to zero. The factor $\beta' (0 < \beta' < 1)$ is the multiplier of the uncracked concrete shear stiffness, G, which accounts for the reduced shear stiffness after cracking has resulted from dowel action and aggregate interlock, and is called the "shear retention factor". It should be noted that in the rotating crack model of concrete, the numerical simulation of cracking is not greatly influenced by shear retention factor. To model the tension-stiffening effect using the descending branch of the tensile stress-strain curve, E_1 is determined as the secant modulus of elasticity.

The cracking models employed in conjunction with the smeared crack procedure can be

categorized into the following three groups: (1) Fixed crack models, (2) Rotating crack models, and (3) Multiple orthogonal crack models. The analysis of shear wall specimens represented herein, have been performed utilizing rotating crack model. In rotating crack models, the cracking direction is taken to be perpendicular to the current major principal strain at any stage of loading. The stiff response resulting from fixing the principal directions is eliminated by using this model.

3.2.2. Compressive strength degradation after cracking

While cracking takes place, the concrete parallel to the crack direction is still capable of resisting tensile or compressive stresses. If it is subjected to tension, a linear elastic behavior for concrete is assumed up to a tensile stress level equal to the tensile strength of concrete, f_t', which represents the onset of the linear softening branch of tensile stress-strain curve of concrete.

However, when concrete is subjected to compression, the damages caused to the concrete with the transverse post-cracking tensile strains, have a degrading effect not only on the compressive

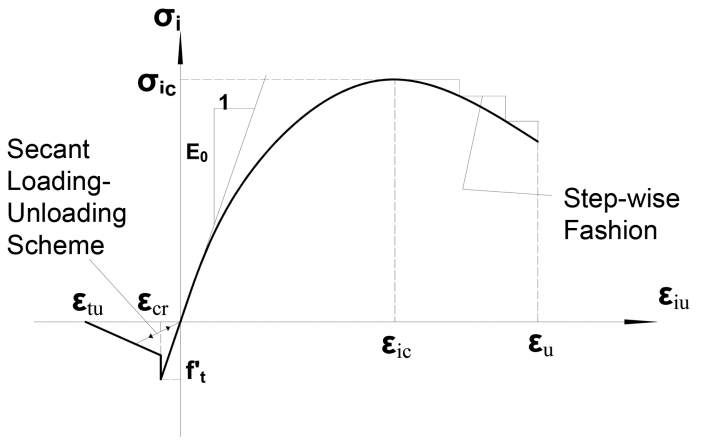

(a) Plain concrete

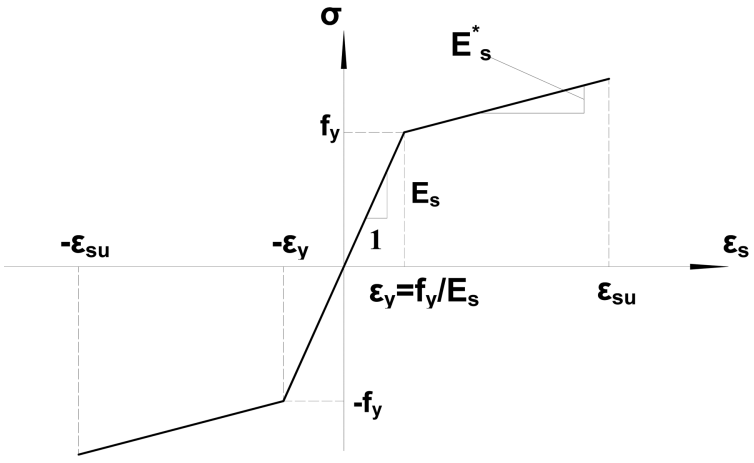

(b) Steel reinforcement

Fig. 3 Uniaxial stress-strain curve

strength of the concrete, but also on its compressive stiffness. The following formulas (Vecchio and Collins 1986) are used to determine the degraded compressive strength of the concrete, σ_{2c}, and the associated compressive strain, ε_{2c}:

$$\sigma_{2c} = \frac{f_c'}{\beta} \quad , \quad \varepsilon_{2c} = \frac{\varepsilon_c}{\beta} \quad , \beta = \max\left\{1 \ , \ 0.8 + 0.34\frac{\varepsilon_{1u}}{\varepsilon_c}\right\} \tag{8}$$

Here, ε_{1u} is the current tensile strain in principal direction 1 and ε_c is the uniaxial concrete strain at the peak stress.

3.3. Stress-strain curve of concrete

An analytical expression which represents the stress-strain curve of a cylinder of concrete subjected to monotonically increasing compressive loads up to failure should be employed in the model. The following relationship (Thorenfeldt, *et al.* 1987) is able to accurately represent the family of stress-strain curves for different strength concretes including the high strength concrete is adopted. This expression relating the stress, σ_i, and the equivalent uniaxial strain caused by this stress, ε_{iu}, is introduced as (Fig. 3(a)):

$$\frac{\sigma_i}{\sigma_{ic}} = \frac{n_i \dfrac{\varepsilon_{iu}}{\varepsilon_{ic}}}{n_i - 1 + \left(\dfrac{\varepsilon_{iu}}{\varepsilon_{ic}}\right)^{n_i k_i}} \tag{9}$$

Where: σ_i = current compressive principal stress in principal direction i, ε_{iu} = equivalent uniaxial strain resulted from σ_i, σ_{ic} = compressive strength of biaxially loaded concrete resulting from the failure envelope curve, ε_{ic} = equivalent uniaxial strain when σ_i reaches σ_{ic}, n_i = curve fitting factor in principal direction i, and k_i = factor to increase the post peak decay in stress. Here, k_i is equal to 1 when $\varepsilon_{iu}/\varepsilon_{ic}$ is less than 1, and it is a number greater than 1 when $\varepsilon_{iu}/\varepsilon_{ic}$ exceeds 1. Collins and Porasz (1989) suggested the value of k_i for $\varepsilon_{iu}/\varepsilon_{ic} > 1$ as $k_i = 0.67 + \sigma_{ic}/62$. The parameter n_i takes a value greater than 1 and is evaluated using the equation: $n_i = 0.8 + \sigma_{ic}/17$. In the computer program if the calculated value for n_i is less than or equal to 1, it is assigned a value of 1.1. Eq. (9) makes the relationship between σ_i and ε_{iu} as a function of four constants: σ_{ic}, ε_{ic}, n_i and k_i. These four constants can all be obtained from the compressive strength of the concrete, σ_{ic}, which is evaluated from the failure envelope curve suggested by Kupfer and Gerstle (1973) depending on the biaxial loading ratio ($\alpha = \sigma_1/\sigma_2$). If the initial slope E_0 of the stress-strain curve (initial modulus of elasticity) is known, or it can be estimated, the strain at peak stress ε_{ic} can be found from $\varepsilon_{ic} = \sigma_{ic} \cdot n_i/(E_0 \cdot (n_i - 1))$. The initial tangent stiffness of the concrete, E_0, lies between the stiffness of the aggregate and the stiffness of the paste; it can be estimated by using experimental relationships. The values of E_1 and E_2 required in Eq. (2) for a given stress ratio ($\alpha = \sigma_1/\sigma_2$) are found as the slopes of the $\sigma_1 - \varepsilon_{1u}$ and $\sigma_2 - \varepsilon_{2u}$ curves, respectively. The tangent to the ascending branch of the stress-strain curve, Eq. (9), is given by $E_i = d\sigma_i/d\varepsilon_{iu}$. For the elastic tension region (ascending branch of tensile stress-strain curve), E_i is assumed to be equal to E_0 and for the descending branch of the compression zone, E_i is set equal to zero to avoid computational difficulties associated with a negative value for E_i. The value of E_i in this region is given by the user and the unbalanced stresses are released in a step-wise fashion. In descending branch of the tension zone, the secant stiffness model was employed. See Fig. 3(a).

3.4. Equivalent Poisson's ratio

Concrete under uniaxial and biaxial compression first compacts and then dilatates due to the internal microcracking. To take this dilatancy of concrete into account the value of the equivalent Poisson's ratio is assumed to be of the following form (Ottosen 1979):

$$\nu = \begin{cases} \nu_i & \gamma_2 \le \gamma_a \\ \nu_f - (\nu_f - \nu_i)\sqrt{1-\left(\dfrac{\gamma_2-\gamma_a}{1-\gamma_a}\right)^2} & \gamma_2 > \gamma_a \end{cases} \tag{10}$$

in which, ν_i is the initial Poisson's ratio; γ_2 is the nonlinear index which represents the ratio of the actual compressive stress, σ_2, to the corresponding value of that stress at failure (ultimate strength), σ_{2c}, ($\gamma_2 = \sigma_2/\sigma_{2c}$); ν_f is the Poisson's ratio at failure and set equal to 0.36; and γ_a is the nonlinear index corresponding to the onset of dilatancy which is set to be 0.80; because the Poisson's ratio starts to increase at the stress level corresponding to $\gamma_a = 0.8$ (Kupfer, *et al.* 1969). In the model, an upper bound $\nu \le 0.45$ is set to eliminate problems associated with the Poisson's ratio approaching 0.5; theoretically, material with $\nu \ge 0.5$ are uncompressible. For the tension-tension stress condition, $\nu = \nu_i$, is applicable. The initial Poisson's ratio, ν_i, is assumed to be equal to 0.20.

3.5. Failure criteria for concrete

Behavior of concrete under biaxial stress states, as reported by a number of investigators is remarkably different from that under uniaxial conditions. Based on the experimental observation

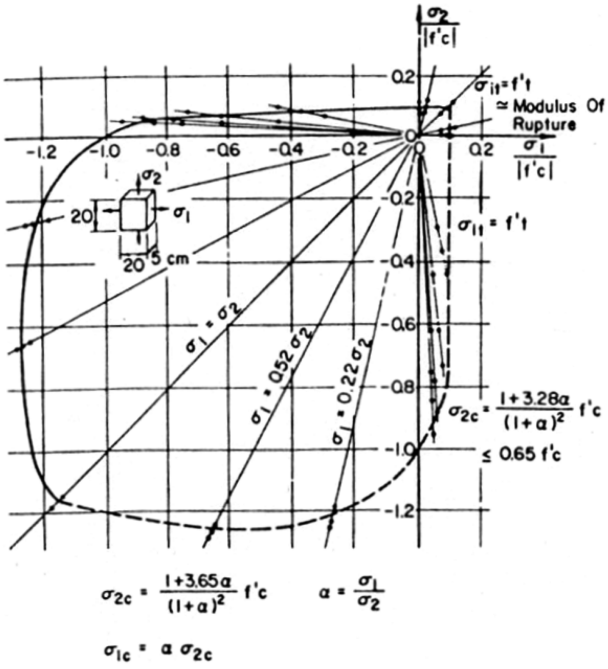

Fig. 4 Typical biaxial failure envelope for concrete (Ghoneim 1978)

under biaxial compression, the compressive strength of the concrete increases because of the internal friction and aggregate interlock. Conversely, a lateral compressive stress decreases the tensile strength of the concrete because the compressive stress introduces tensile stresses at the micro-level due to the heterogeneity of the material which increases the process of internal damage as reported by Vonk (1990). A lateral tensile stress has no major influences on the tensile strength of concrete. To account for these phenomena, the failure envelope proposed by Kupfer and Gerstle (1973), is employed to obtain the compressive and tensile strength of concrete under the biaxial stress state. The lateral tensile stress beyond cracking can also decrease the compressive strength of concrete as obtained by Vecchio and Collins (1986), and Feenstra and de Borst (1993). To account for this, the model proposed by Vecchio and Collins (1986) is used in the proposed formulation as discussed earlier. The biaxial strength envelope curve developed (Fig. 4) by Kupfer, *et al.* (1969) is used in the program built up in the present study.

3.6. Constitutive relationship for steel reinforcement

The behavior of steel reinforcement is basically uniaxial and consequently modeling of its behavior is relatively simple compared to that of the concrete. Two aspects of steel models are relevant here; the representation of steel in the finite element model and the constitutive relationship. The three most common methods used to represent reinforcing steel in finite element models are: (1) Distributed (smeared) model, (2) Embedded model, and (3) Discrete model. Program can use both distributed and embedded model for steel reinforcements. The steel reinforcement is treated in HODA program as an elasto-plastic-strain-hardening material as shown in the Fig. 3(b).

3.7. Nonlinear finite element formulation

The history and capabilities of HODA program are extensive and can be found in literature, e.g. see Shayanfar (1995). But in quick view, this program can depict, through the entire monotonically

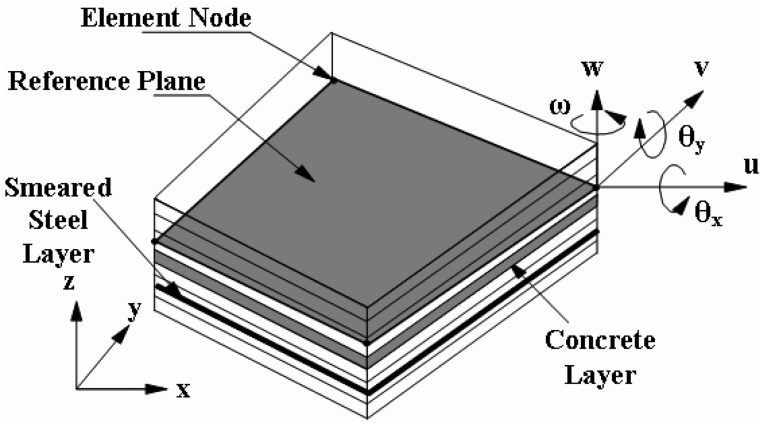

Fig. 5 Facet shell element and associated degree of freedoms

increasing load range, the static and reversed cyclic response of any plain, reinforced or prestressed concrete structure that is composed of thin plate members. This includes beams, slabs (plates), shells, folded plates, box girder, shear walls, or any combination of these structural elements. Time-dependent effects such as creep and shrinkage can be also studied. The element library includes

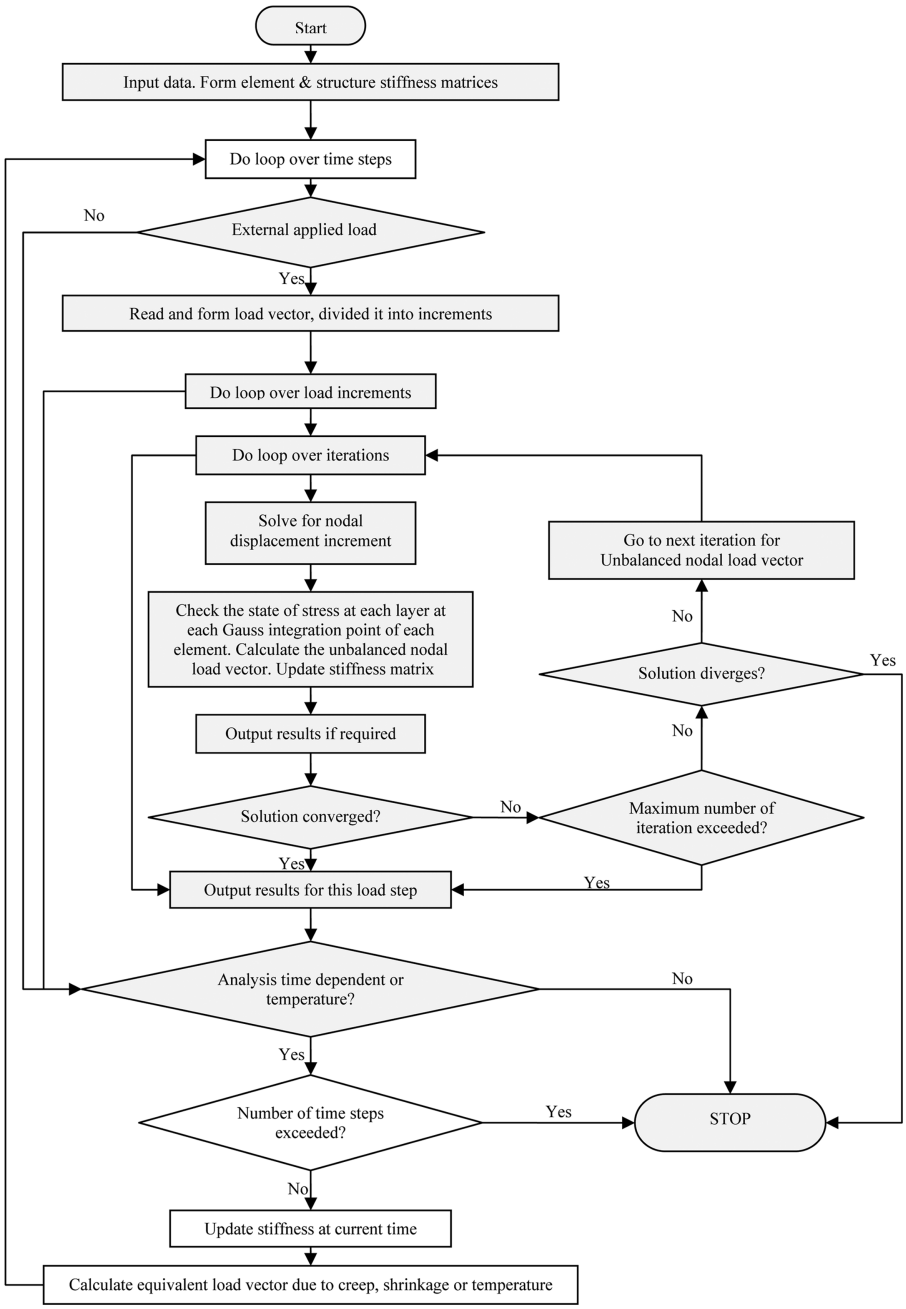

Fig. 6 Solution procedures flowchart

membrane, plate bending, facet shell, one-dimensional bar, and boundary elements. Fig. 5 shows facet element which has been used for modeling the RC walls. The program employs a layered finite element approach. The structure is idealized as an assemblage of thin constant thickness plate elements with each element subdivided into a number of imaginary layers. Each layer is assumed to be in plane stress condition, and can be in any state - uncracked, partially cracked, fully cracked, non-yielded, yielded, and crushed - depending on the stress or strain conditions. Analysis is performed using an incremental-iterative tangent stiffness approach, and the stiffness of the element is obtained by adding the stiffness contributions of all layers at each Gauss quadrature point. The incremental-iterative procedure with a tangent stiffness scheme has been adopted in HODA program. Convergence criteria are utilized to stop the iterations in each load step as soon as a required degree of accuracy has been attained. In the HODA program, two convergence criteria are adopted: (1) absolute values of input convergence/divergence data, and (2) convergence/ divergence criteria that uses input percentage factors to be multiplied by the solutions computed in the first iteration of each load step. For any of these procedures two possible convergence criteria are used: "the force convergence criterion" and "the displacement convergence criterion". As for the convergence criteria, two possible divergence criteria are also available in the HODA program. The program solution procedures are explained by a flowchart in Fig. 6. This program was recently developed further to account for reinforced concrete members with corroded reinforcements (Shayanfar, *et al.* 2007, Shayanfar and Safiey 2008).

4. Comparison of predictions and experimental results

4.1. Reinforced concrete shear panel, W-2

The shear panel W-2, tested by Cervenka (1970) under monotonically increasing load, is investigated in this example. The panel consists of orthogonally reinforced square plates, 762×762 mm^2 (30×30 in^2) in size, and 76.2 mm (3 in) in thickness. Two panels are combined to form one beam like the specimen shown in Fig. 7. The material properties of the shear panel are summarized in Table 1. Because of symmetry, only one-half of the specimen is idealized for the finite element analysis. The wall is divided into 80 rectangular finite elements for analysis using the HODA program (see Fig. 8). Plane stress conditions are assumed, and therefore, a finite element consisting of one layer of concrete is sufficient. The total load is applied at the two points on the outer rib as shown in Fig. 8. The horizontal and vertical reinforcements are represented by smeared steel layers; but, the vertical reinforcements of the ribs are modeled using discrete bar elements and are lumped in single bars at the reference surfaces. A 4×4 Gauss quadrature is used for estimating the integrations involved. The material properties of the concrete and the reinforcing steel used are the same as those used in the experiment and are presented in Table 1. The value of ε_{tu} for each mesh size is calculated by the program using the proposed model to eliminate the mesh size dependency draw back; the details of the model are discussed elsewhere by Shayanfar, *et al.* (1997).

The analytical load-deflection curve for the shear panel W-2 is compared with experimental results in Fig. 9. The initiation of cracks predicted by the analytical model agrees well with the experimental findings as shown in Fig. 9. It can be observed from the load-deflection curves shown in Fig. 9 that the analytical responses exhibit flexible behavior in comparison to the experimental response at load levels beyond 85 kN after initiation of cracks. It is very difficult to attribute this

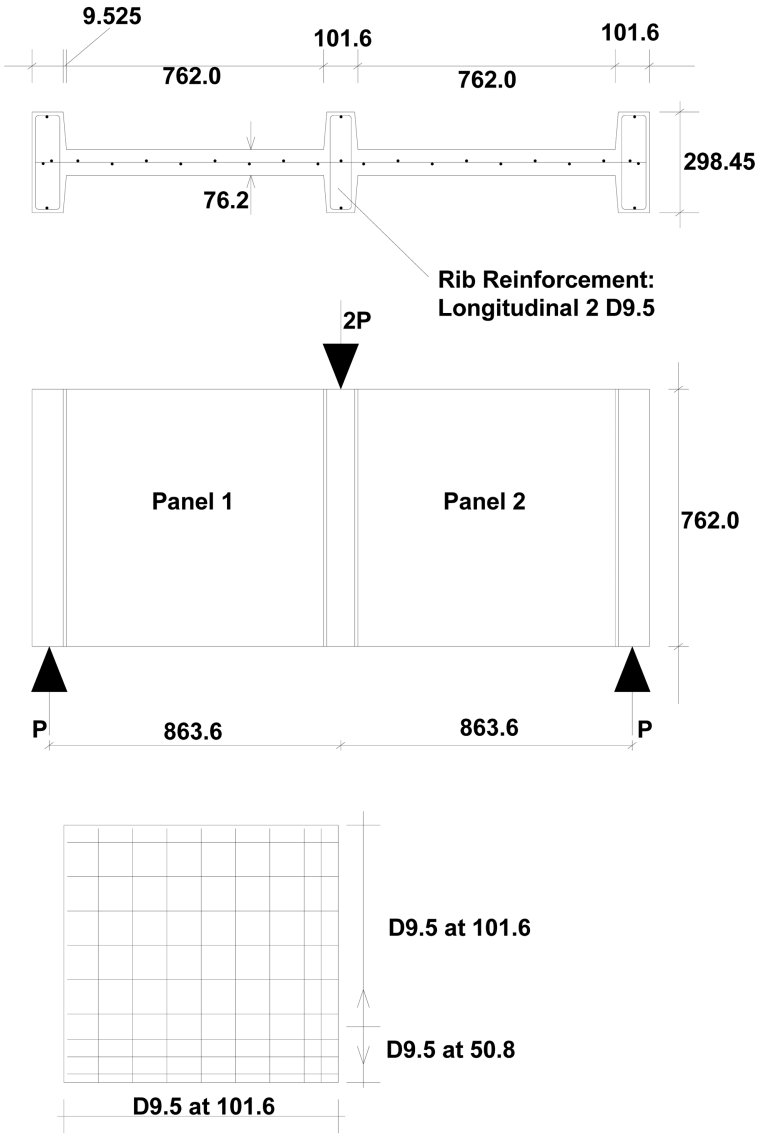

Fig. 7 Details of reinforcements and geometry for shear panel W-2 (Cervenka 1970)

decreased stiffness to any single parameter, but it is likely to be caused by the employed “tension stiffness” model; the descending branch of concrete tensile stress-strain curve in a simple manner was assumed as a straight line. However, upon the initiation of the yielding of specimens, the load-deflection curve follows the experimental response closely until the failure of the panel. The ultimate load predicted by the HODA program is 117 kN, which is only 0.76% lower than the experimental ultimate load of 117.9 kN. The ultimate mid-span deflection predicted by the HODA program is 11.7 mm, which is 23% higher than the experimental ultimate deflection of 9.5 mm (See Table 2). The initial stiffness of the analytical load-deflection curve is 157.93 kN/mm, which is 5.6% softer than the experimental value (167.32 kN/mm).

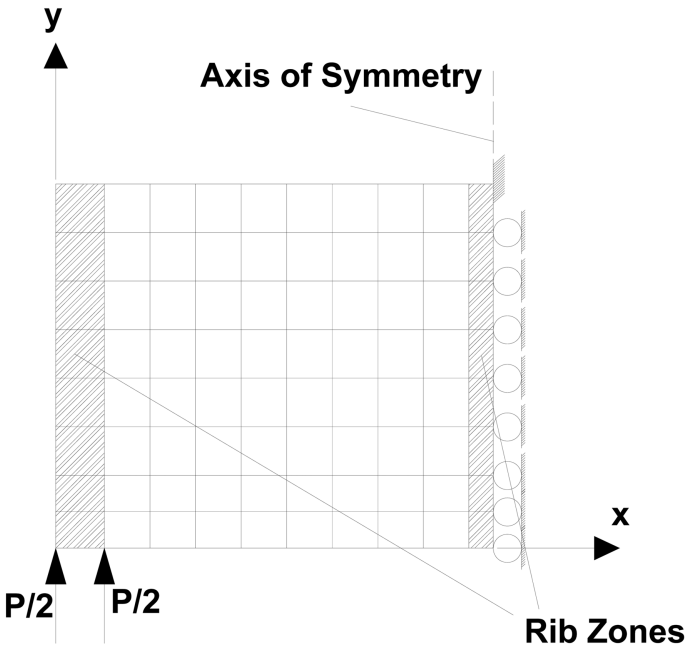

Fig. 8 Mesh configuration for shear panel W-2 (80 elements)

Table 1 Material properties of reinforced concrete walls

Material Properties	W-2	DP1		DP2		SW21	SW22	SW25	SW26
		Web and Flange Walls	Top Slab	Web and Flange Walls	Top Slab				
f_c', MPa	25.16	21.7	43.9	18.8	38.0	36.38	43.01	38.25	25.59
f_t', MPa	3.654	2.5	4.0	1.7	2.1	1.99†	2.16†	2.04†	1.67†
E_0, MPa	19996.0	25900.0	36800.0	18580.0	26414.0	30158.0†	32791.0†	30923.0†	25291.0†
ε_c	0.0025	0.00212	0.00196	0.00212	0.00196	0.003†	0.003†	0.003†	0.003†
ε_u	0.0035†	0.0035†	0.0035†	0.0035†	0.0035†	0.01†	0.01†	0.01†	0.01†
f_y, MPa	353.02	605.0	550.0	605.0	550.0	470.0 (d_1=8.0) 520.0 (d_2=6.25) 420.0 (d_3=4.0)	470.0 (d_1=8.0) 520.0 (d_2=6.25) 420.0 (d_3=4.0)	420.0 (d_1=4.0) 520.0 (d_2=6.25) 470.0 (d_3=8.0)	470.0 (d_1=8.0) 520.0 (d_2=6.25) 420.0 (d_3=4.0)
E_s, MPa	188230.0	190250.0	219120.0	190250.0	219120.0	213745.0†	213745.0†	213745.0†	213745.0†
ε_{su}	0.036	0.0883	0.1†	0.0883	0.1†	0.13†	0.13†	0.13†	0.13†

†=assumed value

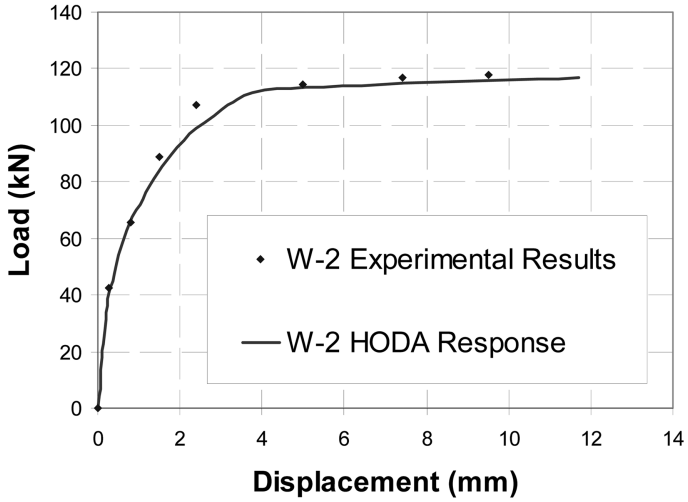

Fig. 9 Load-deflection curve for shear panel W-2

Table 2 Comparisons between the analytical and the experimental results

	Ultimate lateral load bearing capacity			Final lateral displacement		
	Experimental, kN	Analytical, kN	Error, %	Experimental, mm	Analytical, mm	Error, %
W-2	117.9	117.0	0.76	9.5	11.7	23.0
DP1	1298.0	1200.0	7.6	15.0†	15.2	1.3
DP2	904.0	840.0	7.1	10.0†	10.7	7.0
SW21	127.4	117.0	8.2	22.0	21.8	0.9
SW22	152.0	152.0	0.0	16.38	13.8	15.75
SW25	149.5	148.0	1.0	9.87	12.8	29.69
SW26	122.0	116.0	5.0	22.0	28.5	29.5

†=at this displacement, the test was halted.

4.2. The squat shear walls, DP1 and DP2

The reliability of the proposed material model under monotonic load conditions once more is examined by analysis of more complicated specimens. For this purpose, the shear walls, namely, DP1 and DP2, tested by Palermo and Vecchio (2002) under reversed cyclic loading are undertaken. The walls system consisted of three isotropically and orthogonally reinforced square plates to form an I-shape shear wall which are connected to a slab and a foundation in top and bottom, respectively. The geometry of the walls is shown in Fig. 10; as it can be seen, the wall systems consist of two flange walls and one web wall. The horizontal cyclic displacement is applied to top slab which is transmitted to the walls. Two walls were tested in a similar way, but DP1 test was designed with constant vertical loading and DP2 without it. The material properties of the concrete and the steel reinforcement are given in Table 1. Also, the reinforcement layout of wall systems can be found in Fig. 11; the slabs were reinforced with No.30 deformed reinforcing bars at a spacing

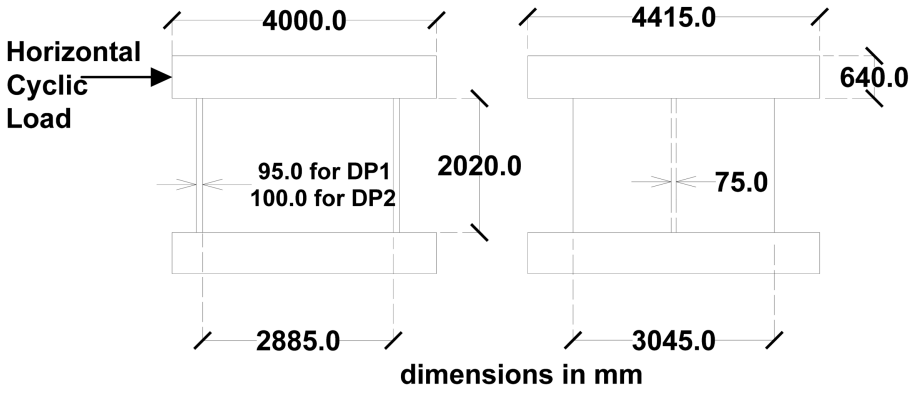

Fig. 10 Details of DP series specimens (Palermo and Vecchio 2002)

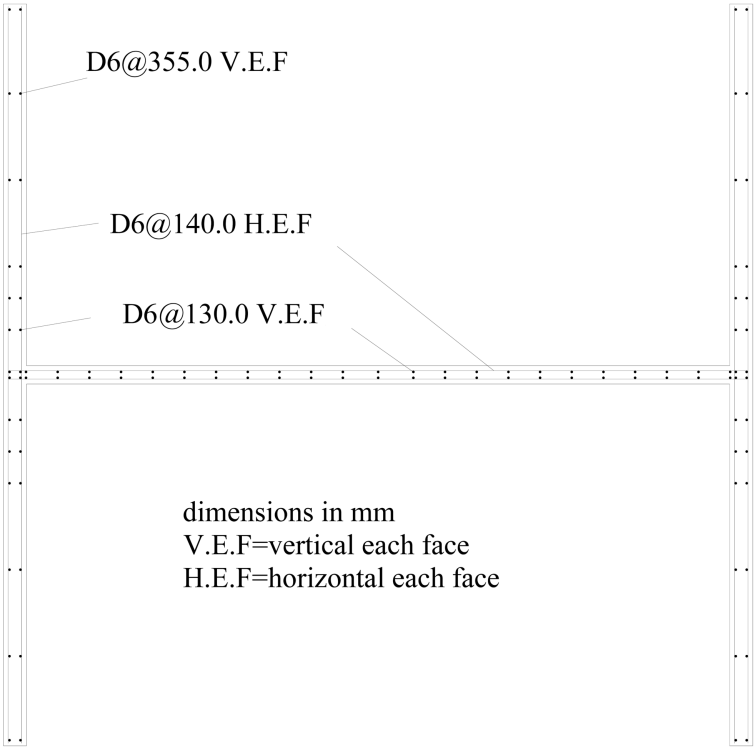

Fig. 11 Reinforcing layout of walls (Palermo and Vecchio 2002)

350 mm in top and bottom layers in two ways. The walls are discretized into 220 shell elements as shown in Fig. 12. Three types of elements can be considered, namely: web, flange, and top slab elements. The slab of foundation was not considered in modelings due to the small effect of this part to the total behavior of the wall systems; but, not considering such a thick mat foundation in the finite element representative model could affect the location of the failure. Since layered finite element technique has been employed; therefore, four layers of concrete for walls and one layer for top slab are considered. The distributed reinforcement in the web and flanges and top slab are

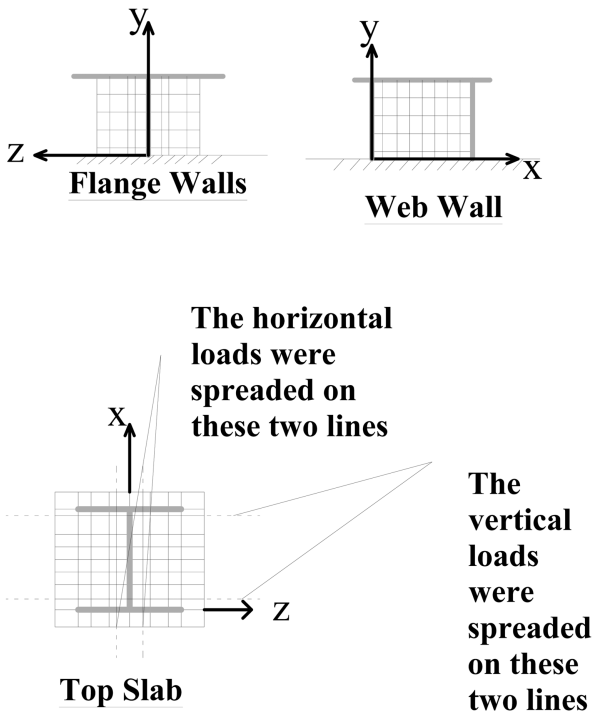

Fig. 12 Details of DP series finite element idealization

idealized as two smeared steel layers. A 4×4 Gauss-quadrature grid are used for numerical computation of the involved integrations. The total applied axial load for DP1, including weight of the top slab, was 1200 kN. 940 kN was applied on the top slab which is identically simulated in modeling as shown in Fig. 12; this load was spread on two lines which represents the positions of load spreader beams in experiment. No Axial load was applied to DP2 model according to experiment design. The total horizontal loads are applied at the two rows of points on mid plane of top slab as shown in Fig. 12, in monotonic form; the loadings were not applied in concentrated form to evade some possible local failures resulting in sudden total failure of specimen. The monotonic loads are applied in maximum 30 load steps with a maximum of 15 iterations per load step. As suggested by Palermo and Vecchio (2004), the compressive cylinder strength of last row of elements both in web and flanges near to top slab and the other associated characteristics are reduced by a factor of 30% for the specimen DP2. The monotonic analytical envelope curves have been compared with first excursion positive displacement experimental envelope curves as shown in Fig. 13**.** The ultimate load bearing capacities of the DP1 and DP2 are computed by program as 1200.0 and 840.0 kN, respectively. The estimated capacities have only 7.6% and 7.1% differences from the experimental ones, as indicated in Table 2. The initial stiffness of analytical load-deflection curves for specimens DP1 and DP2 are 461.25 kN/mm and 347 kN/mm, respectively; which, have 4.6% and 0.6% toleration in comparison to the experimental stiffness (441.0 kN/mm for DP1, and 349.0 kN/mm for DP2). It was observed from experimental results that the presence of an axial constant load significantly enriches the ductility of the shear dominated reinforced concrete wall (Palermo and Vecchio 2002). This may be attributed to the beneficial effects of axial compressive

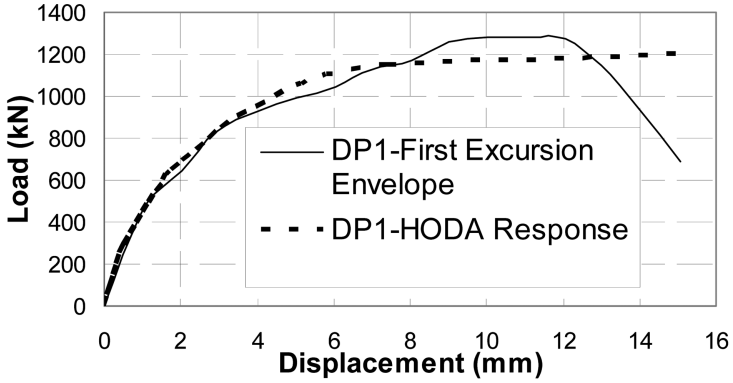

(a) DP1

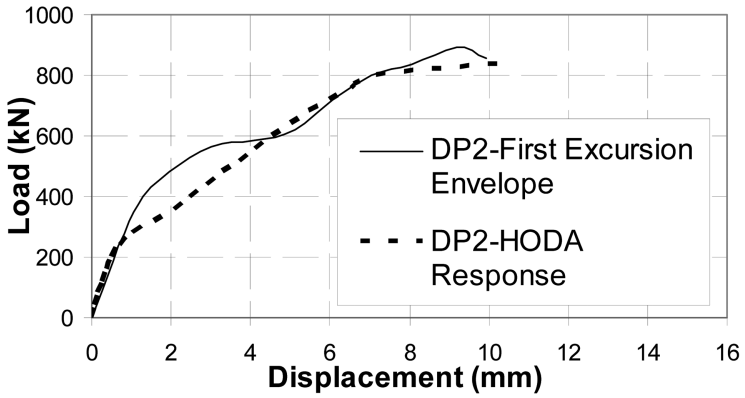

(b) DP2

Fig. 13 Comparisons between the monotonic response of program and first excursion experimental envelope curve

load on the shear capacity of these types of the specimens-although it should be noted that the specimen DP2 failed prematurely due to weaker concrete near the top of the wall. A comparison between computer program predictions of load-deformation curve for specimens (DP1 and DP2) and experimental findings show that this phenomenon has been anticipated reasonably by the proposed constitutive model.

The results presented for the shear walls DP1 and DP2 further represent the reliability of the computer program in handling the nonlinear finite element analysis.

4.1. Reinforced concrete shear walls, SW 21, SW22, SW25, and SW26

Four experimental shear wall specimens, tested by Lefas, *et al.* (1990), at Imperial College under monotonically increasing load, were selected for analysis. The four test specimens are referred to as SW21, SW22, SW25 and SW26. Material properties are given in Table 1. Typical details of reinforcing, geometry, mesh configuration and experimental loading diagram for all specimens are shown in Fig. 14. The SW22 and SW25 specimens are affected by constant axial loads (N) in

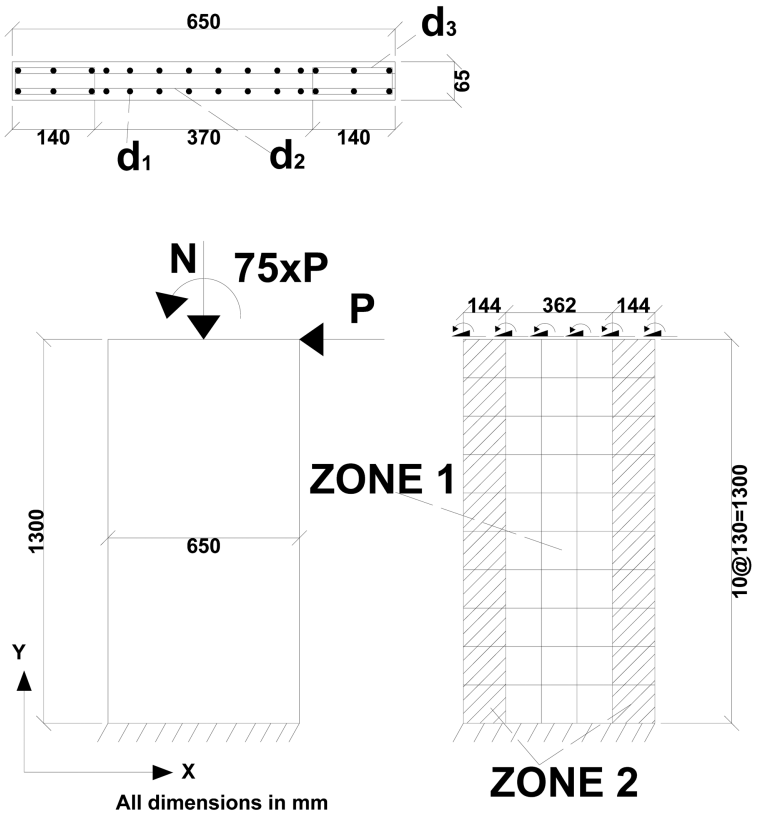

Fig. 14 SW shear walls; structural details, and finite element representative model

addition to lateral load (*P*), which are equal to 182 and 325 kN, respectively. An upper beam with depth of 150.0 mm had been adjoined to the top of the shear walls in the experimental test setup, and the monotonically increasing lateral load had been applied to the middle of it. It is ignored in the modeling, and consequently a moment had been applied simultaneously with lateral load as shown in the Fig. 14. The steel reinforcing was modeled with smeared steel layers in two directions. The analytical results are compared with experimental results in Table 2. This reveals the good correlations between the experimental results and the program predictions.

5. Conclusions and summary

The analytical study undertaken in this research program is aimed at developing a simple material model applicable for any types of concrete structures under different types of loadings. All of the features for concrete are included in the material model developed during the course of this study. A new hypoelasticity model is developed based on the concept of equivalent uniaxial strain utilizing the rotation of the material axis during subsequent iteration/ load step. The Popovics' stress-strain curve is modified for application into the above hypoelastic material model. A simple model is utilized to remedy the mesh dependency drawback from nonlinear FE analysis of RC structures. A study is carried out on modeling and analysis of DP series structural

shear walls and W-2 shear panels to verify the performance of the proposed models. Finally, the accuracy of the established relationships is further validated by modeling and analyses of SW shear walls.

Notation

$[C]$ = constitutive matrix in local coordination
d_i = reinforcement diameter, i=1,2, and 3
E_0 = intial moduli of elasticity of concrete
E_i = tangent moduli in prinicipal direction i; i=1,2
E_s = intial tangent moduli for reinforcing steel
E_s^* = tangent modulus for reinforcing steel in strain hardening region
f_y = yield strength of reinforcing steel
f_c' = concrete uniaxial compressive sterngth
f_t' = concrete uniaxial tensile strength
G = shear modulous
k_i = factor to increase post-peak decay
n_i = curve fitting factor
N, P = load
u, v, w = translational degrees of freedom
α = stress ratio
β = a parameter associated to compressive strength degragation model
β' = shear retension factor
ε = strain
ε_c = concrete starin at peak stress
ε_{cr} = cracking strain of concrete
ε_i = strain corresponding to σ_i
ε_{ic} = equivalent uniaxial strain corresponding σ_{ic}
ε_{ij} = normal strains i=j, i=1,2
ε_{iu} = equivalent uniaxial strain in ith direction; i=1,2
$\varepsilon_{i,\,ju}$ = equivalent uniaxial strain in ith direction due to stress in jth direction; i, j=1,2 and $i \neq j$
ε_s = steel reinforcement strain
ε_{su} = ultimate strain at rupture for reinforcing steel
ε_y = steel strain at yield
ε_{tu} = ultimate uniaxial tensile strain of concrete
ε_u = ultimate uniaxial compressive strain of concrete
γ_{12} = enginnering shear strain
γ_2 = nonlinear index used in equivalent Poisson's ratio
γ_a = nonlinear index corresponding to the onset of dilatancy used in equivalent Poisson's ratio
θ = angle between the old coordinate system and the new coordinate system
θ_{old}, θ_{new} = old or new angle between the local coordinate system and the principal coordinate system
$\Delta\theta_i$ = the angle between the current pricipal coordinate system and the previous coordinate system
θ_x = plate normal rotation about x-axis
θ_y = plate normal rotation about y-axis

ν = equivalent Poisson's ratio
ν_i = initial Poisson's ratio
ν_{ij} = Poisson's ratio in ith direction due to uniaxial loading in jth direction; i, j=1,2
ν_f = final Poisson's ratio
σ = stress
$\sigma_1(\sigma_2)$ = major(minor) principal stress
σ_i =principal stress, i=1, 2
σ_{ic} = compressive strength of biaxially loaded concrete in direction i, i=1,2
σ_{ij} = normal stresses i=j, i=1,2
τ_{12} = shear stress
ω = drilling degree of freedom in membrane element

References

ASCE Publication (1982), *Finite Element Analysis of Reinforced Concrete*, A. H. Nilson, eds., American Society of Civil Engineering, New York, USA.

ASCE Publication (1985), *Finite element analysis of RC structures*, C. Meyer, and H. Okamura, eds., American Society of Civil Engineering, New York, USA.

Balan, T. A., Spacone, E. and Kwon, M. (2001), "A 3D hypoplastic model for cyclic analysis of concrete structures", *Eng. Struct.*, **23**, 333-342.

Bathe, K. J., Walczak, J., Welch, A., and Mistry, N. (1989), "Nonlinear analysis of concrete structures", *Comput. Struct.*, **32**, 563-590.

Bouzaiene, A. and Massicotte, B. (1997), "Hypoelastic tridimensional model for nonproportional loading of plain concrete", *J. Eng. Mech.*, **123**(11), 1111-1120.

Cervenka, V. (1970), "Inelastic finite element analysis of reinforced concrete panels under in-plane loads", PhD Dissertation, Department of Civil Engineering, University of Colorado, CO.

Collins, M. P. and Porasz, A. (1989), "Shear strength for high strength concrete", *Bull. No. 193*, Design Aspects of High Strength Concrete, Committee Euro-International du Beton, 75-83.

Darwin, D. and Pecknold, D. (1974), "Inelastic model for cyclic biaxial loading of reinforced concrete", *SRS No.409*, University of Illinois, USA.

Elwi, A. A. and Murray, D. W. (1979), "A 3D hypoelastic concrete constitutive relationship", *J. Eng. Mech. Div., ASCE*, **105**(EM4), 623-641.

Feenstra, P. H. and de Borst, R. (1993), "Aspects of robust computational modeling for plain and reinforced concrete", *Heron Pub.*, **38**(4).

Ghoneim, G. A. M. (1978), "Nonlinear analysis of concrete structures", PhD Dissertation, Department of Civil Engineering, University of Calgary, Calgary, Canada.

Kupfer, H. B., Hildsdorf, H. K., and Ruch, H. (1969), "Behavior of concrete under biaxial stresses", *ACI J.*, **66**(8), 656-666.

Kupfer, H. B. and Gerstle, K. H. (1973), "Behavior of concrete under biaxial stresses", *J. Struct. Div., ASCE*, **48**(EM), 852-866.

Kwak, H. G. and Kim, D. Y. (2001), "Nonlinear analysis of RC shear walls considering tension-stiffening effect", *Comput. Struct.*, **79**, 449-517.

Kwak, H. G. and Kim, D. Y. (2004a), "Material nonlinear analysis of RC shear walls subject to monotonic loadings", *Eng. Struct*, **26**, 1517-1533.

Kwak, H. G. and Kim, D. Y. (2004b), "Material nonlinear analysis of RC shear walls subject to cyclic loadings", *Eng. Struct.*, **26**, 1423-1436.

Lefas, I. D., Kotsovos M. D., and Ambraseys, N. N. (1990), "Behavior of reinforced concrete structural walls: strength, deformation characteristic, and failure mechanism", *ACI Struct. J.*, **87**(1), 23-31.

Ottosen, N. S. (1979), "Constitutive model for short-time loading of concrete", *J. Eng. Mech. Div.*, **105**(1), 127-141.

Palermo, D. and Vecchio, F. J. (2002), "Behavior of three-dimensional reinforced concrete shear walls", *ACI Struct. J.*, **99**(1), 81-89.
Palermo, D. and Vecchio, F. J. (2004), "Compression field modeling of reinforced concrete subjected to reverse cyclic loading: Verification", *ACI Struct. J.*, **101**(2), 155-164.
Rashid, Y. R., (1968), "Ultimate strength analysis of prestressed concrete pressure vessels", *Nuclear Eng. Design*, **7**(4), 334-344.
Shayanfar, M. A. (1995), "Nonlinear finite element analysis of normal and high strength concrete structures", PhD Dissertation, Department of Civil Engineering and Applied Mechanics, McGill University, Montreal, Canada.
Shayanfar, M. A., Ghalehnovi, M., and Safiey, A. (2007), "Corrosion effects on tension stiffening behavior of reinforced concrete", *Comput. Concrete*, **4**(5), 403-424.
Shayanfar, M. A., Kheyroddin, A., and Mirza, M. S. (1997), "Element size effects in nonlinear analysis of reinforced concrete members", *Comput. Struct.*, **62**, 339-352.
Shayanfar, M. A. and Safiey, A. (2008), "A new approach for nonlinear finite element analysis of reinforced concrete structures with corroded reinforcements", *Comput. Concrete*, **5**(2), 155-174.
Thorenfeldt, E., Tamaszemicz, A., and Jenson, J. J. (1987), "Mechanical properties of high strength concrete and application in design", *Proceedings of International Symposium on Utilization of High Strength Concrete*, Stanvanger, Norway, 149-159.
Vecchio, F. J. and Collins, M. P. (1986), "The modified compression field theory for reinforced concrete elements subjected to shear", A*CI Struct. J.*, **83**(2), 219-231.
Vonk, R. A. (1990), "Softening response of concrete loaded in compression", PhD Dissertation, Eindhoven University of Technology, The Netherlands.

CC